Sprays," *Twentieth Symposium (International) on Combustion*, Combustion Inst., Pittsburgh, PA, 1984, pp. 1283–1290.

[3]Ball, G. J., and Pratt, N. H., "Laser Induced Fluorescence Imaging of Interphase Mass Transfer in Steam/Water Flows," *Proceedings of the VI International Conference Photon Correlation and Other Techniques in Fluid Mechanics*, Inst. of Physics Conf. (Cambridge, England, UK), Serial 77, Session 3, 1985, pp. 111–116.

[4]Allen, M. G., and Hanson, R. K., "Digital Imaging of Species Concentration Fields in Spray Flames," *Twenty-First Symposium (International) on Combustion*, Combustion Inst., Pittsburgh, PA, 1986, pp. 1755–1761.

[5]Hancock, R. D., Jackson, T. A., and Nejad, A. S., "Technique for Visualizing Vaporlines Emanating from Water Droplets," *Applied Optics*, Vol. 31, No. 9, 1992, pp. 1163–1166.

[6]Chen, L.-D., and Roquemore, W. M., "Visualization of Jet Flames," *Combustion and Flame*, Vol. 66, No. 1, 1986, pp. 81–86.

[7]Switzer, G. L., "A Versatile System for Stable Generation of Uniform Droplets," *Review of Scientific Instruments*, Vol. 62, No. 11, 1991, pp. 2765–2771.

[8]Welch, J. E., Harlow, F. H., Shannon, J. P., and Daly, B. J., "The MAC Method, a Computing Technique for Solving Viscous, Incompressible Transient Fluid Involving Free Surface," Los Alamos Scientific Lab., Rept. LA-3425, Los Alamos, NM, 1966.

[9]Hirt, C. W., and Cook, J. L., "Calculating Three-Dimensional Flows Around Structures and Over Rough Terrain," *Journal of Computational Physics*, Vol. 10, No. 2, 1972, p. 324–340.

[10]Boris, J. P., Oran, E. S., Fritts, M. J., and Oswald, C. E., "Time Compressible Similarities of Shear Flows," Naval Research Lab., NRL Memo Rept. 5249, Washington, DC, 1983.

[11]Chan, R. K. C., Street, R. L., and Strelkoff, T., "Computer Studies of Finite Amplitude Water Waves," Stanford Univ., Dept. of Civil Engineering, TR 104, Stanford, CA, 1969.

[12]Clift, R., Grace, J. R., and Weber, M. E., *Bubbles, Drops, and Particles*, Academic Press, San Diego, CA, 1978, Chap. 5.

Effect of Partial Thickness Actuation on Stress Concentration Reduction near a Hole

Pradeep K. Sensharma,* Mohammad H. Kadivar,† and Raphael T. Haftka‡
Virginia Polytechnic Institute and State University, Blacksburg, Virginia 24061

Introduction

RECENTLY, there has been much interest in adaptive structures that can respond to a varying environment by changing their properties. Piezoelectric materials and shape memory alloys (SMA) are often used as partial thickness actuators to create such adaptivity by applied energy, usually electric current.[1,2] These actuators can be used to induce strains in a structure and reduce stresses in regions of high stress concentration.

Two of the present authors showed that axisymmetric actuation strains applied throughout the thickness of a plate with a hole can reduce the stress concentration factor (SCF) in an isotropic plate from 3 to 2 (Ref. 3). However, in most cases actuators are expected to be bonded to or embedded in the plate, so that the actuation strains are applied in the actuators and not directly in the plate.

The objective of this Note is to show that such partial-thickness actuation cannot be used to reduce the stress concentration factor with axisymmetric actuation strain distribution.

Received April 14, 1993; revision received Sept. 27, 1993; accepted for publication Sept. 27, 1993.

*Graduate Research Assistant, Department of Aerospace and Ocean Engineering. Student Member AIAA.

†Visiting Professor, Shiraz University, Shiraz, Iran.

‡Christopher C. Kraft Professor, Department of Aerospace and Ocean Engineering. Associate Fellow AIAA.

Problem Definition

A plate with a small hole under uniaxial tensile loading (S) with a ring of bonded and embedded actuators is shown in Fig. 1. The plate is treated analytically as an infinite plate. The radial, tangential, and shear-stress distribution for this case are given by[4]

$$\sigma_r^M = \frac{S}{2}\left[1-\left(\frac{A}{r}\right)^2\right]+\frac{S}{2}\left[1+3\left(\frac{A}{r}\right)^4-4\left(\frac{A}{r}\right)^2\right]\cos 2\theta \tag{1}$$

$$\sigma_\theta^M = \frac{S}{2}\left[1+\left(\frac{A}{r}\right)^2\right]-\frac{S}{2}\left[1+3\left(\frac{A}{r}\right)^4\right]\cos 2\theta \tag{2}$$

$$\tau_{r\theta}^M = -\frac{S}{2}\left[1-3\left(\frac{A}{r}\right)^4+2\left(\frac{A}{r}\right)^2\right]\sin 2\theta \tag{3}$$

where A is the radius of the hole. In Ref. 3, our goal was to reduce the stress concentration as measured by Von-Mises or maximum shear-stress criteria by adding axisymmetric actuation strain fields with the piezoelectric actuators placed near the hole. The actuators account for only part of the thickness of the plate, being either bonded or embedded to the plate in the vicinity of the hole. Bonded and embedded actuators are shown in Fig. 1, where t_a is the thickness of each actuator and t_p is the thickness of the plate.

The total stresses at radius r are given as

$$\sigma_r^{\text{tot}} = \sigma_r^M + \sigma_r^I, \quad \sigma_\theta^{\text{tot}} = \sigma_\theta^M + \sigma_\theta^I \tag{4}$$

where σ_r^I and σ_θ^I are the radial and tangential stresses due to the actuator action, respectively. The Von-Mises equivalent stress is given by

$$\sigma_{\text{eq}} = \sigma_V = \sqrt{\sigma_1^2 - \sigma_1\sigma_2 + \sigma_2^2} \tag{5}$$

where σ_1 and σ_2 are the principal stresses calculated from the total stress components. The equivalent stress based on the maximum shear-stress criterion is given by

$$\sigma_{\text{eq}} = \sigma_{MS} = |\sigma_1 - \sigma_2| \tag{6}$$

when σ_1 and σ_2 are of the opposite sign. When σ_1 and σ_2 carry the same sign, then

$$\sigma_{\text{eq}} = \sigma_{MS} = \max(|\sigma_1|, |\sigma_2|) \tag{7}$$

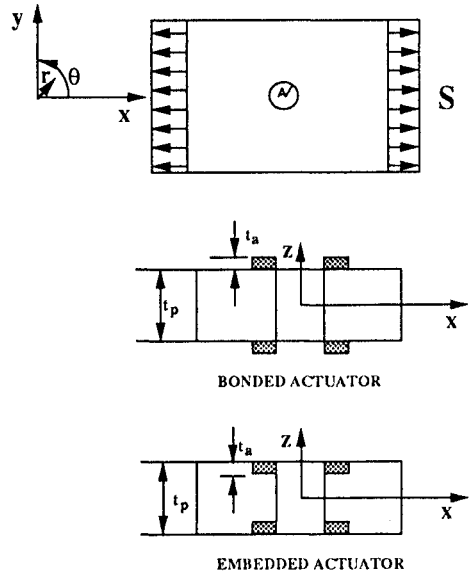

Fig. 1 Bonded and embedded actuators near the hole.

The stress concentration factor is defined as the ratio of the maximum equivalent stress to the applied stress (i.e., σ_{eq}/S).

Analysis

The radial and tangential strains due to the actuator action in the plate and in the actuators can be written as

$$\varepsilon_r^I = \frac{1}{E}(\sigma_r^I - \nu\sigma_\theta^I) + \varepsilon_r^i, \quad \varepsilon_\theta^I = \frac{1}{E}(\sigma_\theta^I - \nu\sigma_r^I) + \varepsilon_\theta^i \tag{8}$$

where ε_r^i, ε_θ^i are the radial and tangential actuation strains, respectively. Note that the actuation strains and the resulting stresses are not constant through the thickness. However, we assume that the actuation regions are symmetric through the thickness and that the strains are constant through the thickness. Integrating Eqs. (8) through the thickness and dividing by the total thickness t_T, where

$$t_T = 2t_a + t_p \tag{9}$$

we get

$$\varepsilon_r^I = \frac{1}{t_T E^*}(N_r^I - \nu N_\theta^I) + \varepsilon_r^*, \quad \varepsilon_\theta^I = \frac{1}{t_T E^*}(N_\theta^I - \nu N_r^I) + \varepsilon_\theta^* \tag{10}$$

where E^* is the average Young modulus, i.e.,

$$E^* = \frac{1}{t_T}\int_{-(t_T/2)}^{t_T/2} E\, dz = \frac{2t_a E_a + E_p t_p}{t_T} \tag{11}$$

and ε_r^*, ε_θ^* are the average radial and tangential actuation strains, respectively, i.e.,

$$\varepsilon^* = \frac{1}{t_T}\int_{-(t_T/2)}^{t_T/2} \varepsilon^i(z)\, dz \tag{12}$$

In the present study, we assume that we have constant actuation strain in the actuator ($\varepsilon^i = \varepsilon_a^i$) and none in the plate, so that

$$\varepsilon^* = \frac{2t_a}{t_T}\varepsilon_a^i = \beta\varepsilon_a^i \tag{13}$$

N_r^I, N_θ^I are the stress resultants

$$N_r^I = \int_{-(t_T/2)}^{t_T/2} \sigma_r^I\, dz, \quad N_\theta^I = \int_{-(t_T/2)}^{t_T/2} \sigma_\theta^I\, dz \tag{14}$$

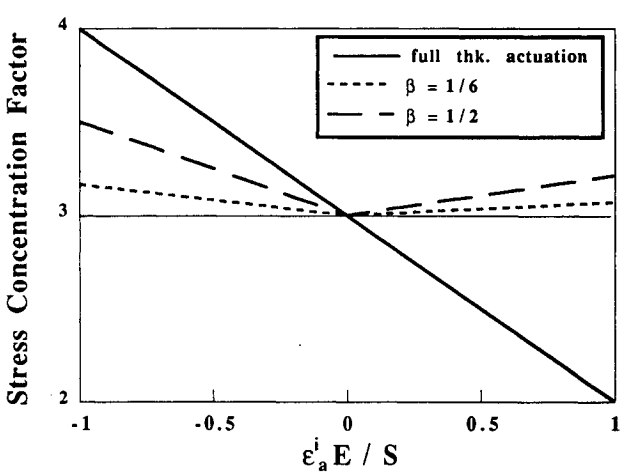

Fig. 2 Effect of full- and partial-thickness actuation on stress concentration factor of the plate near the edge of the hole at θ = 90 deg and ν = 0.3 (maximum shear-stress criterion).

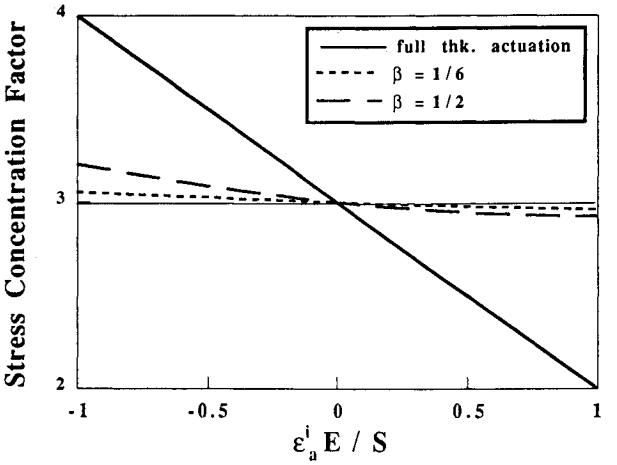

Fig. 3 Effect of full- and partial-thickness actuation on stress concentration factor of the plate near the edge of the hole at θ = 90 deg and ν = 0.3 (Von Mises stress criterion).

For axisymmetric response, the compatibility equation can be written as

$$\varepsilon_\theta^I - \varepsilon_r^I + r\frac{d\varepsilon_\theta^I}{dr} = 0 \tag{15}$$

and the equilibrium equation as

$$N_\theta^I = \frac{d}{d}(rN_r^I) \tag{16}$$

Substituting for ε_r^I and ε_θ^I from Eqs. (10) and making use of the equilibrium equation, we obtain the compatibility equation in the following form:

$$r\frac{d}{dr}\left[\frac{1}{r}\frac{d}{dr}(r^2 N_r^I)\right] = -t_T E^* r\frac{d\varepsilon_\theta^*}{dr} - t_T E^*(\varepsilon_\theta^* - \varepsilon_r^*) \tag{17}$$

Integrating the above equation with free edge boundary conditions at $r = A$ and at $r \to \infty$, we obtain

$$N_r^I = -\frac{t_T E^*}{r^2}\int_A^r \varepsilon_\theta^* \rho\, d\rho - \frac{t_T E^*}{r^2}\int_A^r\int_A^{\rho_1}\frac{\rho_1}{\rho}(\varepsilon_\theta^* - \varepsilon_r^*)\, d\rho\, d\rho_1$$
$$+\frac{t_T E^*}{2}\int_A^r \frac{(\varepsilon_\theta^* - \varepsilon_r^*)}{\rho}\, d\rho - \frac{t_T E^* A^2}{2r^2}\int_A^r \frac{(\varepsilon_\theta^* - \varepsilon_r^*)}{\rho}\, d\rho \tag{18}$$

and substituting N_r^I in the equilibrium equation, we get

$$N_\theta^I = -t_T E^* \varepsilon_\theta^* + \frac{t_T E^*}{r^2}\int_A^r \varepsilon_\theta^* \rho\, d\rho$$
$$+\frac{t_T E^*}{r^2}\int_A^r\int_A^{\rho_1}\frac{\rho_1}{\rho}(\varepsilon_\theta^* - \varepsilon_r^*)\, d\rho_1\, d\rho - t_T E^*\int_A^r \frac{(\varepsilon_\theta^* - \varepsilon_r^*)}{\rho}\, d\rho$$
$$+\frac{t_T E^*}{2}\int_A^r \frac{(\varepsilon_\theta^* - \varepsilon_r^*)}{\rho}\, d\rho + \frac{t_T E^*}{2r^2}A^2\int_A^r \frac{(\varepsilon_\theta^* - \varepsilon_r^*)}{\rho}\, d\rho \tag{19}$$

Equating ε_r^i and ε_θ^I from Eqs. (8) and (10) and solving for σ_r^I and σ_θ^I, we get

$$\sigma_r^I = \frac{E}{t_T E^*}N_r^I + \frac{E}{1-\nu^2}[(\varepsilon_r^* - \varepsilon_r^i) + \nu(\varepsilon_\theta^* - \varepsilon_\theta^i)] \tag{20}$$

$$\sigma_\theta^I = \frac{E}{t_T E^*} N_\theta^I + \frac{E}{1-\nu^2}\left[\nu\left(\varepsilon_r^* - \varepsilon_r^i\right) + \left(\varepsilon_\theta^* - \varepsilon_\theta^i\right)\right] \tag{21}$$

where N_r^I and N_θ^I are given by Eqs. (18) and (19). For the axisymmetric isotropic actuation with constant actuation strain in the actuator, i.e., ε_r^i and $\varepsilon_\theta^I = \varepsilon_a^i$, and zero actuation strain in the plate, the expressions for the stresses simplify. In the actuators, we get

$$\sigma_{ra}^I = -\frac{E}{r^2}\int_A^r \varepsilon^* \rho \, d\rho + \frac{E\left(\varepsilon^* - \varepsilon_a^i\right)}{1-\nu}$$

$$\sigma_{\theta a}^I = \frac{E}{r^2}\int_A^r \varepsilon^* \rho \, d\rho + \frac{E\left(\nu\varepsilon^* - \varepsilon_a^i\right)}{1-\nu} \tag{22}$$

while in the plate we get

$$\sigma_{rp}^I = -\frac{E}{r^2}\int_A^r \varepsilon^* \rho \, d\rho + \frac{E\varepsilon^*}{1-\nu}$$

$$\sigma_{\theta p}^I = \frac{E}{r^2}\int_A^r \varepsilon^* \rho \, d\rho + \frac{\nu E\varepsilon^*}{1-\nu} \tag{23}$$

These equations were compared with finite element calculations and close agreement was observed.

Note that Eqs. (22) and (23) predict nonzero radial stresses at the hole boundary, $r = A$. This incorrect prediction is due to the two-dimensional analysis. Thus, we can expect that the above equations provide reasonable results only at a small distance away from the hole. For the full thickness, we have only actuators and $\beta = 1$ and the induced stresses are obtained from Eqs. (22) as

$$\sigma_r^i = -\frac{E}{r^2}\int_A^r \varepsilon^i \rho \, d\rho, \quad \sigma_\theta^i = \frac{E}{r^2}\int_A^r \varepsilon^i \rho \, d\rho - E\varepsilon^i \tag{24}$$

The above stress expressions for the full-thickness actuation are the same as those obtained in Ref. 3.

Discussion

The mechanical stresses in the plate peak at the edge of the hole at $\theta = 90$ deg where $\sigma_\theta = 3S$ for a stress concentration factor of 3. The variation of stress concentration factor in the plate near the edge of the hole at $\theta = 90$ deg with normalized actuation strains for full-thickness and partial-thickness actuations are shown in Figs. 2 and 3 for maximum shear stress and Von-Mises stress criteria, respectively.

In the case of full-thickness actuation, when positive actuation strains are applied, it can be seen from Eqs. (24) that the induced stresses are compressive. Also, the induced tangential stresses are quite large in magnitude compared to the induced radial stresses. These induced stress distributions can produce large reduction in the total tangential stresses at the edge of the hole and the stress concentration factor. Figures 2 and 3 confirm the results obtained in Ref. 3 that the stress concentration can be reduced from 3 to 2 (at which point $\theta = 0$ deg becomes critical in compression).

For partial-thickness actuation, the situation is different because of the large radial stresses generated in the plate. Two partial-thickness actuation cases of bonded actuators are shown. For $\beta = 1/6$, the actuator thickness is small compared to the thickness of the plate. In the second case, the thicknesses of the actuators and plate are the same, i.e., $\beta = 1/2$. For both cases, the induced stress distributions are completely different from that obtained with the full-thickness actuation. We can see from Eqs. (23) that near the hole the radial induced stress is larger than the induced tangential stress by a factor of $1/\nu$. When we apply negative actuation strains, the induced radial stresses in the plate increase near the edge of the hole. This increases the stress concentration factor for both criteria, as shown in Figs. 2 and 3, even though the total tangential stress decreases. Positive actuation strains, on the other hand, induce tensile stresses in the plate, and as we can see from Fig. 2, the SCF based on maximum shear-stress criterion increases with the applied actuation strains. However, the SCF based on the Von-Mises stress criterion, as can be seen from Fig. 3, decreases as we increase the applied actuation strain. But the decrease in stress concentration factor with partial-thickness actuation is quite small compared to the full-thickness actuation case. Similar results were obtained with embedded actuators also. Stresses in the actuators are similar to those obtained in the plate for the full-thickness actuation.

Thus, it can be seen that the partial-thickness actuation is ineffective for axisymmetric distribution. This is due to the large radial stresses produced by the actuators. This is in marked contrast to the full-thickness actuation (Ref. 3) where the stress concentration factor could be reduced from 3 to 2 by axisymmetric distributions. Thus, with partial-thickness actuation stress concentration reduction can be achieved only with asymmetric actuation.[5]

Acknowledgments

This research was supported by U.S. Army Research Office Grant DAAL03-92-G-0180 and NASA Grant NAG-1-168.

References

[1]Lin, M. W., and Rogers, C. A., "Analysis of Stress Distribution in a Shape Memory Alloy Composite Beam," AIAA Paper 91-1164-CP; see also *Proceedings of the AIAA/ASME/ASCE/AHS/ASC 32nd Structures, Structural Dynamics, and Materials Conference*, Part 1, AIAA, Washington, DC, 1991, pp. 169–177.

[2]Crawley, E. F., and de Luis, J., "Use of Piezoelectric Actuators as Element of Intelligent Structures," *AIAA Journal*, Vol. 25, No. 10, 1987, pp. 1373–1385.

[3]Sensharma, P. K., Palantera, M. J., and Haftka, R. T., "Stress Reduction in an Isotropic Plate with a Hole by Applied Induced Strains," *Proceedings of the AIAA/ASME/ASCE/AHS/ASC 33rd Structures, Structural Dynamics, and Materials Conference*, Part 2, AIAA, Washington, DC, 1992, pp. 905–913 (AIAA Paper 92-2525).

[4]Timoshenko, S. P., and Goodier, J. N., *Theory of Elasticity*, 3rd ed., McGraw Hill, New York, 1951, Chap. 4.

[5]Sensharma, P. K., and Haftka, R. T., "Limit of Stress Reduction in a Plate with a Hole using Piezoelectric Actuators," *Proceedings of the 1993 ASME Winter Annual Meeting* (New Orleans, LA), Vol. 35, Nov. 1993, pp. 157–164.

Buckling and Vibration Analysis of Skew Plates by the Differential Quadrature Method

X. Wang,* A. G. Striz,† and C. W. Bert‡
University of Oklahoma, Norman, Oklahoma 73019

Introduction

THERE are no known closed-form solutions for the buckling and free vibration behavior of skew plates. Therefore, numerical methods must be utilized to solve the problem. The most widely used ones are various Rayleigh-Ritz methods, the Galerkin method, the finite element method, the finite strip method, the finite difference method, and the Lagrangian multiplier method. Although the Rayleigh-Ritz method uses less computational effort

Received March 3, 1993; revision received Aug. 10, 1993; accepted for publication Aug. 10, 1993.

*Visiting Assistant Professor, School of Aerospace and Mechanical Engineering; currently at the Aircraft Engineering Department, Nanjing University of Aeronautics and Astronautics, Nanjing, People's Republic of China.

†Associate Professor, School of Aerospace and Mechanical Engineering, 865 Asp Avenue. Associate Fellow AIAA.

‡Director and Perkinson Chair Professor, School of Aerospace and Mechanical Engineering, 865 Asp Avenue. Fellow AIAA.